Journal of Power Sources 225 (2013) 257–262

Contents lists available at SciVerse ScienceDirect

Journal of Power Sources

journal homepage: www.elsevier.com/locate/jpowsour

Extension lifetime for dye-sensitized solar cells through multiple dye adsorption/desorption process

Yi-Fang Chiang [a], Ruei-Tang Chen [b], Po-Shen Shen [a], Peter Chen [a,c,*], Tzung-Fang Guo [a,c,**]

[a] Department of Photonics, National Cheng Kung University, Tainan, Taiwan 701, ROC
[b] Department of Electro-Optical Engineering, Southern Taiwan University of Science and Technology, Tainan, Taiwan 701, ROC
[c] Advanced Optoelectronic Technology Center, National Cheng Kung University, Tainan, Taiwan 701, ROC

HIGHLIGHTS

- A novel concept to extend the photoanodes lifetime is studied and characterized.
- V_{oc} and dye adsorption are enhanced under multiple dye adsorption/desorption process.
- The dyeing kinetics is faster after multiple recycling processes.

GRAPHICAL ABSTRACT

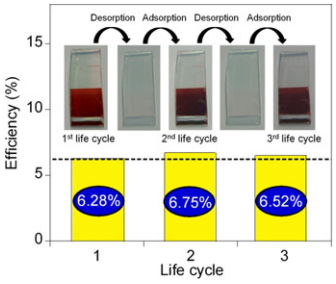

ARTICLE INFO

Article history:
Received 25 June 2012
Received in revised form
18 September 2012
Accepted 13 October 2012
Available online 23 October 2012

Keywords:
Dye-sensitized solar cells
Reliability
Fast dyeing
Extension lifetime

ABSTRACT

In this study, we propose a novel concept of extending the lifetime of dye-sensitized solar cells (DSCs) and reducing the costs of re-conditioning DSCs by recycling the FTO/TiO_2 substrates. The photovoltaic performances of DSCs using substrates with various cycles of dye uptake and rinse off history are tested. The results show that dye adsorption and V_{oc} are significantly increased under multiple dye adsorption/desorption process and resulted in the improvement of power conversion efficiency. Moreover, the dyeing kinetics is faster after multiple recycling processes, which is favorable for the industrial application. With surface analysis and charge transport characteristics, we also demonstrate the optimal functionality of TiO_2/dye interface for the improved V_{oc} and efficiency. The results confirm that the improved performances are due to increased dye loading and dense packing of dye molecules. Our results are beneficial for the understanding on the extension of DSCs lifetime after long-term operation in the application of DSC modules. This approach may also be applied in the replacement of newly synthesized photosensitizes to the active cells.

1. Introduction

Dye-sensitized solar cells (DSCs) with a nanocrystalline structure were first introduced by O'Regan and Grätzel in 1991 [1]. Since then, the majority of DSC research has focused on improving the light-to-electricity conversion efficiency. Recently, the efficiency of DSCs has achieved 12.3% with the combination of co-sensitization and a cobalt-complex redox mediator having more positive redox potential than I^-/I_3^- [2]. For a high efficiency and stable DSC, it is essential to have a robust nanoparticle/dye interface which

* Corresponding author. Department of Photonics, National Cheng Kung University, Tainan, Taiwan 701, ROC. Tel.: +886 6 2757575x63919; fax: +886 62095040.
** Corresponding author. Department of Photonics, National Cheng Kung University, Tainan, Taiwan 701, ROC. Tel.: +886 6 2757575x63914.
E-mail addresses: petercyc@mail.ncku.edu.tw (P. Chen), guotf@mail.ncku.edu.tw (T.-F. Guo).

0378-7753/$ – see front matter © 2012 Elsevier B.V. All rights reserved.
http://dx.doi.org/10.1016/j.jpowsour.2012.10.052

generates and separates charge efficiently with good control in retarding charge recombination [3]. Thus, a number of studies have modified the nanoparticle surface using techniques such as oxygen plasma treatment for enhanced light harvesting [4,5] and wide-bandgap metal oxide treatment for blocking of recombination [6,7]. In addition, controlling the dye adsorption rate and packing density on the mesoporous titania network is also an important issue to increase the light harvesting efficiency (LHE). Bazzan et al. have demonstrated a methodology to manipulate and optimize a saturation limit in dye uptake at TiO_2 surface using desorption/adsorption cycling process [8]. However, DSCs must have long-term stability and retain its functioning after millions of times of turnover for the catalytic cycle (excitation, charge injection and regeneration) for practical use [9–11]. In real application, maintenance of DSC modules may be necessary in case that the sealant is deteriorated, [9,12,13] induces electrolyte leakage and dye molecules desorbs from the titanium oxide (TiO_2) surface caused by H_2O permeation from the atmosphere after long-term exposure to full sunlight [14]. Furthermore, transparent conductive electrode (TCO) which is an energy demanding material during its processing is expensive and responsible for a major part of a module's cost [15,16]. It is of practical interests if the dye and electrolyte can be refilled into the dead module without discarding the FTO substrate (with titania porous layer). Thus, it is important to evaluate the feasibility of recycling the FTO/TiO_2 substrate after multiple dye adsorption and desorption process. Based on the above considerations to extend the DSCs module lifetime after multiple dyes desorption/adsorption cycling, it is the purpose of this work to conduct a series of experiments to examine this novel concept for the reuse of aged DSCs modules' FTO/TiO_2 substrates.

In this work, we show not only the improved efficiency but also the faster dye uptaking processes with increased dye adsorption after multiple DSC life cycles. We also demonstrate a possibility of extending the photoanodes lifetime, three times of the original one, after multiple cycles of dye desorption/adsorption. In addition, it is important to carry out the phenomenon occurred at the interface between TiO_2 and dye under multiple desorption/adsorption process. Thus, we characterize the functionality of TiO_2/dye interface with UV–vis spectroscopy, attenuated total reflectance–Fourier transform infrared spectroscopy (ATR–FTIR), photovoltage and photocurrent transients, and electrochemical impedance. Our results suggest that reusing the FTO/TiO_2 substrate after multiple dye desorption/adsorption cycling is feasible and replacement of newly synthesized photosensitizes is another beneficial aspect of practical utilization. This concept is particularly important in the retrieving of the aged DSC modules under harsh outdoor use.

2. Experimental procedure

2.1. Materials

TiO_2 paste (ETERDSC Ti-2105) was provided from ETERNAL CHEMICAL CO., LTD. Ru dye, *cis*-bis(isothiocyanato) bis(2,2′-bipyridyl-4,4′-dicarboxylato)-ruthenium(II) bis-tetrabutylammonium ($RuL_2(NCS)_2$-2TBA, also known as N719), and fluorine-doped SnO_2 conductive glass (FTO, 10 Ω square^{-1}) were purchased from Solaronix and Nippon Sheet Glass (NSG), respectively. Sodium hydroxide (NaOH) was purchased from Merck.

2.2. Fabrication of DSCs

Dye-sensitized solar cells were fabricated using the following procedure. The TiO_2 paste was cast onto the FTO substrate by the screen-printing method, followed by sintering at 500 °C for 30 min in air to obtain a transparent TiO_2 photoelectrode with the thickness of 5 μm. The mesoporous TiO_2 photoelectrode was immersed in 0.5 mM N719 solution in acetonitrile and tert-butanol (volume ratio 1:1) for 18 h to complete the sensitizer loading. The cells were assembled by dropping an electrolyte containing 0.1 M I_2, 0.6 M 1-propyl-3-methylimidazolium iodide (PMII), 0.1 M LiI, and 0.5 M tert-butylpyridine in 3-methoxypropionitrile onto the substrate. A platinum sheet was used as a counter electrode. This device is called as 1st life cycle and denoted with abbreviated LC1, as shown in Fig. 1. For the desorption of N719 dye molecules from the TiO_2/FTO substrate, the Pt sheet is peeled from the device, and the LC1 were immersed in NaOH [17–19] solutions of 0.1 M in a mixture of ethanol and deionized (DI) water with a 1:1 volume ratio for 2 h. Afterwards, the bare substrates were immersed in N719 solution and assembled again for the 2nd life cycle (LC2). The LC3 and LC4 were repeated with the same procedure.

2.3. Characterization

The devices were characterized by a Keithley 2400 sourcemeter using a mask with an aperture area of 0.09 cm^2 under standard AM 1.5G-filtered irradiation (100 mW cm^{-2}) from an Oriel 91160A 300 W solar simulator. The spectral-mismatch factor of the simulated solar irradiance was corrected by a Schott visible-color glass-filtered (KG5 color filter) Si diode (Hamamatsu S1133) [20]. The UV–vis spectra were measured by a spectrometer (U-4100, Hitachi). The contact angles were measured with an FACE contact angle meter (Kyowa Kaimen Kagaku Co.). The ATR–FTIR spectrum was measured using a Vertex 70 FTIR spectrometer (Bruker) with the Golden Gate diamond single-reflection ATR accessory (Specac). The electrochemical impedance measurements were recorded on an Eco-Chimie Autolab PGSTAT 30 with the frequency response analyser (FRA) 2 module at a sinusoidal perturbation amplitude of 10 mV under dark conditions at −0.68 V in the frequency range of 10 m–100 kHz. The photovoltage and photocurrent transients were observed using an array of white (10 W) and red (3 W) light emitting diodes (LEDs, Cree XLamp). While a white bias light supplied by white LEDs incidented into the sample, a small perturbation is superimposed by a pulse generated by red LEDs. The pulse width was 500 ms. The recombination lifetime was extracted by fitting the photovoltage decays at various background white light intensities under open-circuit condition. The capacitance is calculated from the following equation as $C = \triangle Q/\triangle V$, where $\triangle V$ is

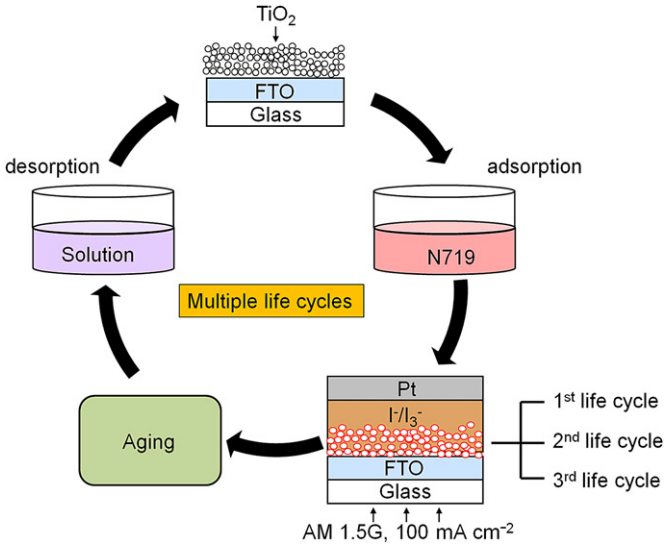

Fig. 1. Schematic illustrations for multiple life cycles on DSCs.

the peak height of transient photovoltage increment from the pulse and $\triangle Q$ is the number of collected electrons (with the same red pulse intensity) integrated by the photocurrent decay under short-circuit condition. The similar measurements were presented elsewhere [21,22].

3. Results and discussion

3.1. Reliability of the DSCs under multiple life cycles

Fig. 2 shows the current–voltage (J–V) characteristic curves of the LC1, LC2, LC3 and LC4. Table 1 and Table S1 show their detailed photovoltaic parameters. LC1 has V_{oc} of 0.68 V, J_{sc} of 12.65 mA cm^{-2}, FF of 0.73, and η of 6.28%. However, the LC2 has a higher power conversion efficiency of 6.75%, which is 7.4% higher than LC1 because of its enhanced V_{oc} of 0.72 V and J_{sc} of 13.24 mA cm^{-2}. LC3 has V_{oc} and J_{sc} values of 0.74 V and 12.26 mA cm^{-2}, respectively, with FF of 0.71 and η of 6.52%. It is noted that although J_{sc} for LC3 is lower than that of LC1, V_{oc} and η are higher. LC4 shows poor performance compared with LC1, which may be ascribed to poor electron transport that resulted from the damages on the TiO_2 surface during multiple desorption processes. Accordingly, the multiple adsorption–desorption results demonstrated that FTO/TiO_2 substrate can survive after manifold dye uptake cycles. More encouragingly, the photovoltaic activity remained vigorous with improvement in power conversion efficiency under practical operation. In order to understand the reason for the increased in V_{oc} and J_{sc}, we will discuss the detail in the following section.

3.2. Variation of dye uptake concentration on TiO_2 surface under multiple life cycles

Fig. 3 shows the UV–vis absorption spectra of the dyed TiO_2 films after various life cycles. The spectrum of the 1st washed off which is desorbed with sodium hydroxide (NaOH) solutions [14–16] for 2 h is also included for comparison. In Fig. 3, the maximum absorption peak for LC1 is around 450–550 nm, which corresponds to the metal-to-ligand charge-transfer (MLCT) transition [18]. The MLCT band of LC1 was completely disappeared after immersing in NaOH solutions. The above results were also true with the desorption process of LC2 and LC3 (as shown in Fig. 1). This observation suggests the total removal of the dye molecules on TiO_2/FTO substrates by NaOH solutions. However, it is worthy to note that a significant increase of MLCT band for multiple life cycles using NaOH solution as desorption agent, indicating increased dye adsorption on the TiO_2 film for LC2 and LC3. The overall integral of the absorption intensity for N719 dye molecules on LC2 and LC3 was enhanced respectively by 42% and 24% as compared to that of LC1. To verify that the adsorption of dye molecules was increased for multiple life cycles, the number of adsorbed dye molecules for LC1 and LC2 was calculated by desorbing the dye molecules from the TiO_2 surface and measuring the absorption spectra in Figure S1 in the supplementary data. The adsorbed N719 dye molecules dissolved in solution from LC2 were found to be increased by 40% compared to that of LC1. The increase in dye absorption of LC2 may result in improved J_{sc} upon multiple life cycles if the sensitizers are chemically adsorbed and can effectively inject light induced electrons.

Table 1
The photovoltaic performance of DSCs for multiple life cycles.

Device	V_{oc} [V]	J_{sc} [mA cm^{-2}]	FF	η [%]
1st life cycle (LC1)	0.68	12.65	0.73	6.28
2nd life cycle (LC2)	0.72	13.24	0.71	6.75
3rd life cycle (LC3)	0.74	12.26	0.71	6.52
4th life cycle (LC4)	0.74	10.94	0.70	5.66

The ATR–FTIR spectra of N719 powder, LC1, and LC2 is shown in Figure S2 in the supplementary data. The peaks located at 1354 cm^{-1} and 1611 cm^{-1} for N719 powder were attributed to $\upsilon_{sym}(COO^-)$ and $\upsilon_{asym}(COO^-)$ stretching, respectively [23–25]. When N719 dye molecules adsorbed onto the TiO_2 surface via a bidentate or bridging linkage, the interaction between dye molecules with TiO_2 causes a shift in $\upsilon_{sym}(COO^-)$ and $\upsilon_{asym}(COO^-)$ [25] stretching to 1373 cm^{-1} and 1601 cm^{-1}, respectively, for LC1 and LC2. Additionally, the peak located at 1714 cm^{-1} (related to C=O stretching) observed for N719 powder was absent for the dyes on film samples. These results suggest that most N719 dye molecules were chemically adsorbed or anchored onto LC1 and LC2. The enhanced adsorption of N719 dye molecules on LC2 evidenced by the UV–vis spectrum corresponding in Fig. 3 can be attributed to denser coverage (chemical adsorption) of N719 dye molecules on the TiO_2 surface for efficient electron injection and back reaction suppression. The aggregation of dye molecules (physical adsorption) had a negligible influence on absorbance.

3.3. Wetting behavior of increased dye adsorption on TiO_2 and the dyeing kinetics under multiple life cycles

As noted above, dye attachment to the TiO_2 surface obviously increased after multiple life cycles. The enhanced dye loading may have resulted from the TiO_2 surface becoming more hydrophilic [4,26]. The insets of Fig. 4(a) and (b) show the contact angle

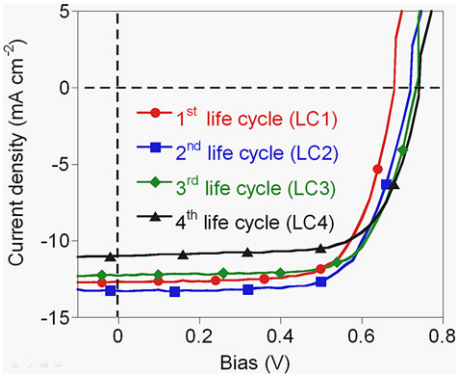

Fig. 2. J–V characteristic curves of (○) 1st life cycle, (□) 2nd life cycle, (◇) 3rd life cycle, and (△) 4th life cycles under the AM 1.5G, 100 mW cm^{-2} illumination.

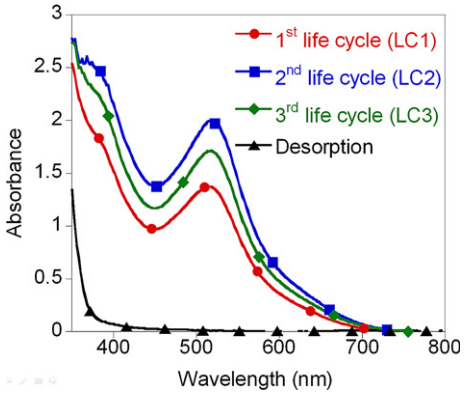

Fig. 3. UV–vis absorption spectra of (○) 1st life cycle and (△) the corresponding sample desorbed with NaOH, (□) 2nd life cycle, (◇) 3rd life cycle.

measurements of water drops on LC1 before dye adsorption (substrate 1) and after dye desorption (substrate 2), respectively. The contact angle of water on substrate 1 is 32°, and that of water on substrate 2 is below 10°. The significant change in the contact angle indicates that the TiO_2 surface becomes very hydrophilic after desorption of dye in NaOH solution. Since the anchoring groups (−COOH) of N719 dye are also hydrophilic, the hydrophilic TiO_2 surface facilitates the interaction of N719 dye molecules with TiO_2 [26]. The TiO_2 surface may have become more hydrophilic due to a change in surface chemistry. It is well known that proton adsorption or desorption on the TiO_2 surface will shift the band edge positions [27,28]. After the desorption process, the surface of TiO_2 becomes deprotonated and negatively charged. In other words, the TiO_2 band edge tends to shift negatively in potential which is beneficial for voltage output.

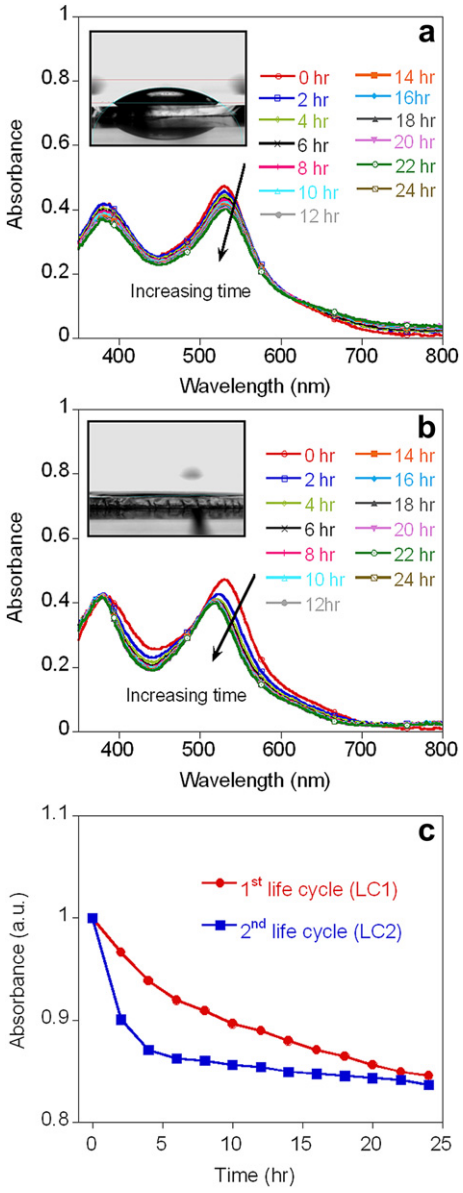

Fig. 4. The absorption variation versus the dipping time for (a) 1st life cycle and (b) 2nd life cycle; (c) dyeing kinetic curves for 1st life cycle and 2nd life cycle. The insets showed the contact angle measurements of water drops on (a) 1st life cycle and (b) 2nd life cycle.

In addition, to verify the effect of the dye adsorption kinetics on substrates, we measure the absorption spectra of N719 solution as a function of TiO_2 immersed time. We inserted the substrate 1 and 2 into individual N719 solution, and measure the decrease of absorbance of N719 solution in specific time interval. The measurement apparatus is presented schematically in Figure S3 in the supplementary data. Fig. 4(a) and 4(b) shows the absorption spectra change of N719 solution inserted with substrate 1 and substrate 2 respectively. Fig. 4(a) shows that the absorbance of N719 solution is gradually decreased with increased dipping time, but there is a significant decrease in the absorbance for the substrate 2 as shown in Fig. 4(b). Interestingly, the maximum absorption peak is blue-shifted in Fig. 4(b) that can be attributed to the deprotonation of N719 [29]. To clearly observe the variance of dye uptaking kinetics, we normalize the absorbance decay as a function of time for the solution with FTO/TiO_2 in the cuvette to the original absorption intensity of the MLCT maximum peak in Fig. 4(c). It is obvious from these two curves, that the dyeing kinetics is faster for substrate 2 than that for substrate 1. This phenomenon is consistent with the fact that the more hydrophilic TiO_2 surface facilitates the interaction of N719 dye molecules with TiO_2 after desorption of dye in NaOH solution as shown in the contact angle images. It is also noted that the absorbance reached a saturated limit for substrate 2 within 6 h. Consequently, this fast dye uptaking process is beneficial in the application of industry to shorten the fabrication time.

3.4. Effects of the improved V_{oc} under multiple life cycles

As mentioned in the previous results, the improved V_{oc} can be observed under multiple life cycles. There are some mechanisms that can result in an increased of V_{oc} such as the suppression of electron back-transfer [6,7] or upward shift of the TiO_2 conduction band [21,30,31] relative to the electrolyte potential. In order to figure out the reasons in improved V_{oc}, photovoltage and photocurrent transient experiments were carried out for the samples to elucidate which mechanisms are dominant. Fig. 5(a) shows the capacitance versus various V_{oc} for LC1 and LC2. In Fig. 5(a), it is shown that no significant differences between LC1 and LC2. These similar curves can be explained as no changes in the band position in TiO_2 after the desorption process. Thus, the increased V_{oc} is unlikely to be ascribed to the up-shift of TiO_2 band edge. Fig. 5(b) presented the recombination lifetime versus V_{oc} for LC1 and LC2. It can be seen that the recombination lifetime is 110 ms for LC2 which is 2 times longer than that for LC1 (56 ms) at V_{oc} = 0.65 V. It suggests a suppression of electron back-transfer from TiO_2 to the electrolyte [32]. This extended electron lifetime may contribute to the improved V_{oc} due to the close-packed coverage of dye molecules on the bare TiO_2 which is also indicated in Fig. 3. Therefore, we believe it is the suppression of electron back-transfer dominated the increased V_{oc} under multiple life cycles rather than the up-shift of TiO_2 band edge. The electrochemical impedance spectrum was performed to confirm this inference.

The charge-transfer process at the interface can be evaluated using electrochemical impedance spectra [33]. Fig. 6 shows the impedance analysis results for LC1 and LC2 under forward bias at darkness. Three semicircles can be observed in the measured frequency range between 10 m and 100 kHz; they are assigned to the resistance at the Pt/electrolyte interface, the resistance of electron back-transfer from TiO_2 to the electrolyte, and the diffusion resistance of I^-/I_3^- in the electrolyte, respectively [34]. In Fig. 6, the diameter of the middle-frequency semicircle of LC2 is larger than that for LC1, which confirms that the resistance for the transfer of electrons from the TiO_2 surface to the electrolyte was higher in LC1. This reduced electron back-transfer kinetics is most likely responsible for the increase in V_{oc}. It is likely that the high packing

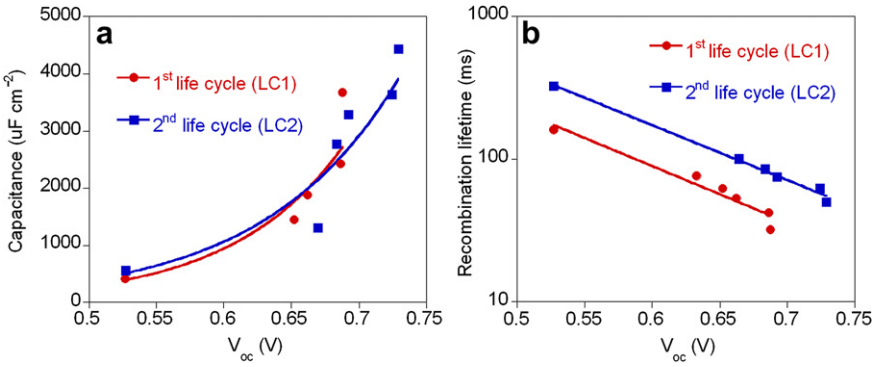

Fig. 5. (a) Capacitance and (b) recombination lifetime versus V_{oc} for 1st and 2nd life cycles.

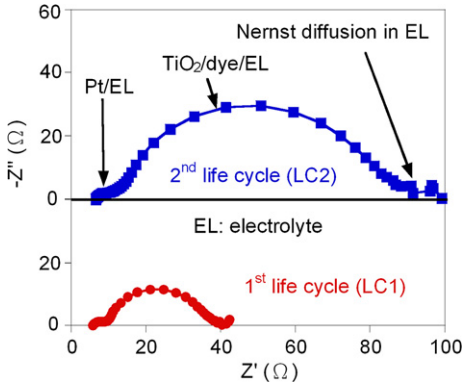

Fig. 6. The electrochemical impedance analysis results (EIS) for (○) 1st life cycle and (□) 2nd life cycle under forward bias in darkness.

density of N719 dye molecular on LC2 may lead to the suppression of recombination between TiO_2/dye and electrolyte interface. Since V_{oc} is associated with the difference between the quasi Fermi level of TiO_2 and the redox potential of the electrolyte [1], the higher V_{oc} could be interpreted by the increased electrons concentrations [31] of the LC2 resulted in the quasi-Fermi level closer to the conduction band.

4. Conclusion

In conclusion, the novel concept of multiple life cycles is proposed in this study. Our results show that DSC substrate remained durable after multiple dye uptake and desorption process. Moreover, the dyeing kinetics is faster after multiple life cycles which is favorable in the industry. With surface and charge transport characteristics, we also figure out the functionality of TiO_2/dye interface for the improved V_{oc}. The suppression of back-electron transfer from TiO_2 to the electrolyte due to the higher coverage of dye molecules on the TiO_2 surface is the main reason for the increase in V_{oc}. This research demonstrates the feasibility of the extension of DSCs lifetime after long-term operation in the application of large DSC modules. The proposed method reduces the costs for recouping DSCs with enhanced performances. This principle may have great interests if we like to replace the 1st life cycle DSC with new photosensitizers of higher conversion efficiency on the original TiO_2/FTO substrates.

Acknowledgments

The authors would like to thank the National Science Council (NSC) of Taiwan (NSC 100-2622-E-006-014-CC2, NSC 99-2113-M-006-009-MY2), and the Asian Office of Aerospace Research and Development (AOARD) (AOARD-10-4054) for financially supporting this research. We thank the ETERNAL CHEMICAL CO., LTD. for supplying us the nanocrystalline TiO_2 paste.

Appendix A. Supplementary data

Supplementary data related to this article can be found at http://dx.doi.org/10.1016/j.jpowsour.2012.10.052.

References

[1] B. O'Regan, M. Grätzel, Nature 353 (1991) 737–740.
[2] A. Yella, H.-W. Lee, H.N. Tsao, C. Yi, A.K. Chandiran, M.K. Nazeeruddin, E.W.-G. Diau, C.-Y. Yeh, S.M. Zakeeruddin, M. Grätzel, Science 334 (2011) 629–634.
[3] B.A. Gregg, F. Pichot, S. Ferrere, C.L. Fields, J. Phys. Chem. B 105 (2001) 1422–1429.
[4] Y. Kim, B.J. Yoo, R. Vittal, Y. Lee, N.-G. Park, K.-J. Kim, J. Power Sources 175 (2008) 914–919.
[5] W.-Y. Wu, T.-W. Shih, P. Chen, J.-M. Ting, J.-M. Chen, J. Electrochem. Soc. 158 (2011) K101–K106.
[6] C.Y. Neo, J. Ouyang, J. Power Sources 196 (2011) 10538–10542.
[7] E. Palomares, J.N. Clifford, S.A. Haque, T. Lutz, J.R. Durrant, J. Am. Chem. Soc. 125 (2003) 475–482.
[8] G. Bazzan, J.R. Deneault, T.-S. Kang, B.E. Taylor, M.F. Durstock, Adv. Funct. Mater. 21 (2011) 3268–3274.
[9] O. Kohle, M. Grätzel, A.F. Meyer, T.B. Meyer, Adv. Mater. 9 (1997) 904–906.
[10] N. Kato, K. Higuchi, H. Tanaka, J. Nakajima, T. Sano, T. Toyoda, Sol. Energy Mater. Sol. Cells 95 (2011) 301–305.
[11] M. Grätzel, C. R. Chim. 9 (2006) 578–583.
[12] M. Amirnasr, M.K. Nazeeruddin, M. Grätzel, Thermochim. Acta 348 (2000) 105–114.
[13] H.G. Agrell, Sol. Energy 75 (2003) 169–180.
[14] J.-H. Yum, R. Humphry-Baker, S.M. Zakeeruddin, M.K. Nazeeruddin, M. Grätzel, Nano Today 5 (2010) 91–98.
[15] K. Onoda, S. Ngamsinlapasathian, T. Fujieda, S. Yoshikawa, Sol. Energy Mater. Sol. Cells 91 (2007) 1176–1181.
[16] P. Li, J. Wu, J.L.M. Huang, Y. Huang, Q. Li, Sol. Energy 83 (2009) 845–849.
[17] K. Hara, Y. Tachibana, Y. Ohga, A. Shinpo, S. Suga, K. Sayama, H. Sugihara, H. Arakawa, Sol. Energy Mater. Sol. Cells 77 (2003) 89–103.
[18] Y.J. Kim, M.H. Lee, H.J. Kim, G. Lim, Y.S. Choi, N.-G. Park, K. Kim, W.I. Lee, Adv. Mater. 21 (2009) 3668–3673.
[19] S. Kambe, K. Murakoshi, T. Kitamura, Y. Wada, S. Yanagida, H. Kominami, Y. Kera, Sol. Energy Mater. Sol. Cells 61 (2000) 427–441.
[20] V. Shrotriya, G. Li, Y. Yao, T. Moriarty, K. Emery, Y. Yang, Adv. Funct. Mater. 16 (2006) 2016–2023.
[21] B.C. O'regan, S. Scully, A.C. Mayer, E. Palomares, J.R. Durrant, J. Phys. Chem. B 109 (2005) 4616–4623.
[22] B.C. O'Regan, K. Bakker, J. Kroeze, H. Smit, P. Sommeling, J.R. Durrant, J. Phys. Chem. B 110 (2006) 17155–17160.
[23] M.K. Nazeeruddin, R. Humphry-Baker, P. Liska, M. Grätzel, J. Phys. Chem. B 107 (2003) 8981–8987.
[24] F. Hirose, K. Kuribayashi, M. Shikaku, Y. Narita, Y. Takahashi, Y. Kimura, M. Niwano, J. Electrochem. Soc. 156 (2009) B987–B990.
[25] C.P. León, L. Kador, B. Peng, M. Thelakkat, J. Phys. Chem. B 110 (2006) 8723–8730.
[26] Y. Kim, C.-H. Yoon, K.-J. Kim, Y. Lee, J. Vac. Sci. Technol. A 25 (2007) 1219–1225.
[27] P. Qu, G.J. Meyer, Langmuir 17 (2001) 6720–6728.
[28] B. O'Regan, L. Xiaoe, T. Ghaddar, Energy Environ. Sci. 5 (2012) 7203–7215.

[29] M.K. Nazeeruddin, S.M. Zakeeruddin, R. Humphry-Baker, M. Jirousek, P. Liska, N. Vlachopoulos, V. Shklover, C.-H. Fischer, M. Grätzel, Inorg. Chem. 38 (1999) 6298–6305.
[30] B.C. O'Regan, J.R. Durrant, P.M. Sommeling, N.J. Bakker, J. Phys. Chem. C 111 (2007) 14001–14010.
[31] D. Cahen, G. Hodes, M. Grätzel, J.F. Guillemoles, I. Riess, J. Phys. Chem. B 104 (2000) 2053–2059.
[32] S. Ito, P. Liska, P. Comte, R. Charvet, P. Péchy, U. Bach, L. Schmidt-Mende, S.M. Zakeeruddin, A. Kay, M.K. Nazeeruddin, M. Grätzel, Chem. Commun. (2005) 4351–4353.
[33] Q. Wang, J.-E. Moser, M. Grätzel, J. Phys. Chem. B 109 (2005) 14945–14953.
[34] C. Longo, A.F. Nogueira, M.-A. De Paoli, H. Cachet, J. Phys. Chem. B 106 (2002) 5925.